Journal of Solid State Chemistry 184 (2011) 2103–2107

Contents lists available at ScienceDirect

Journal of Solid State Chemistry

journal homepage: www.elsevier.com/locate/jssc

Electronic band structures and photovoltaic properties of MWO_4 (M=Zn, Mg, Ca, Sr) compounds

Dong Wook Kim [a,b], In-Sun Cho [c], Seong Sik Shin [a], Sangwook Lee [a,b], Tae Hoon Noh [a], Dong Hoe Kim [a], Hyun Suk Jung [d], Kug Sun Hong [a,b,*]

[a] Department of Materials Science and Engineering, Seoul National University, Seoul 151-744, South Korea
[b] Research Institute of Advanced Materials (RIAM), Seoul National University, Seoul 151-744, South Korea
[c] Department of Mechanical Engineering, Stanford University, Stanford, California 94305, USA
[d] School of Advanced Materials Engineering, Kookmin University, Seoul 136-702, South Korea

ARTICLE INFO

Article history:
Received 18 December 2010
Accepted 5 June 2011
Available online 14 June 2011

Keywords:
Divalent metal tungstate
Electronic band structure
Dye-sensitized solar cell

ABSTRACT

Divalent metal tungstates, MWO_4, with wolframite (M=Zn and Mg) and scheelite (M=Ca and Sr) structures were prepared using a conventional solid state reaction method. Their electronic band structures were investigated by a combination of electronic band structure calculations and electrochemical measurements. From these investigations, it was found that the band structures (i.e. band positions and band gaps) of the divalent metal tungstates were significantly influenced by their crystal structural environments, such as the W–O bond length. Their photovoltaic properties were evaluated by applying to the working electrodes for dye-sensitized solar cells. The dye-sensitized solar cells employing the wolframite-structured metal tungstates ($ZnWO_4$ and $MgWO_4$) exhibited better performance than those using the scheelite-structured metal tungstates ($CaWO_4$ and $SrWO_4$), which was attributed to their enhanced electron transfer resulting from their appropriate band positions.

1. Introduction

Semiconductor photoelectrode materials used in photoelectronic devices, such as photocatalytic [1,2] and photovoltaic systems [3], have attracted considerable attention because the energy conversion efficiency of electronic devices is mainly affected by the electrode materials. For example, the wide band gap semiconductor, TiO_2, has been intensively studied and shown to exhibit high efficiency as the photoelectrode in dye-sensitized solar cells and/or photocatalytic systems, because of its superior optical, photochemical and photoelectronic properties, as well as its chemical stability [3,4]. Recently, however, the development of novel materials [4–7] and the modification of well-known materials [8] for using as efficient photoelectrode materials in photoelectronic devices has been the subject of considerable research for the purpose of further improving the energy conversion efficiency of photoelectronic devices.

Generally, it is believed that the photoelectronic properties of a material are strongly influenced by its crystal structure, and there have been a lot of reports [9–11] on the relationships between the crystal structure and other fundamental properties. From this point of view, i.e. in order to search for efficient photoelectrode materials, it is important to understand not only the various fundamental properties of semiconducting photoelectrode materials, but also their relationships with the other basic properties.

Divalent metal tungstates (MWO_4, M=Ni, Zn, Mg, Ca, Sr and Ba) are known as wide band gap semiconductors with two major crystal structures: wolframite and scheelite. Smaller divalent cations like Mg, Zn and Ni in tungsten compounds favor the construction of the wolframite structure with octahedron coordination, whereas scheelite structures with the tungsten atoms in tetrahedral coordination are formed by larger divalent cations such as Ca, Sr, Ba and Pb.

Yoon et al. [12] reported on the relationships between the crystal structure and the microwave dielectric properties for various divalent metal tungstates. Shan et al. [9] investigated the structure-dependent photocatalytic activity of MWO_4 (M=Ca, Sr and Ba). In addition, divalent metal tungstates have been studied in a variety of applications, such as dielectrics [12,13], humidity sensors [14], catalysts [15], photocatalysts [9,16,17] and laser materials [18,19]. Only a few metal tungstates have been investigated as photoelectrochemical devices [20,21]. Zhao et al. [20] investigated the photocurrent response and photocatalytic activity of porous $ZnWO_4$ films, and Pandey et al. [21] recently reported interesting photoelectrochemical properties using $CuWO_4$ films. However, to the best of our

* Corresponding author. Fax: +82 2 886 4156.
E-mail addresses: dong0414@snu.ac.kr (D.W. Kim), kshongss@plaza.snu.ac.kr (K.S. Hong).

0022-4596/$ - see front matter © 2011 Elsevier Inc. All rights reserved.
doi:10.1016/j.jssc.2011.06.005

knowledge, their application as the photoanode materials for dye-sensitized solar cells has not been reported thus far.

In the present study, divalent metal tungstates, MWO_4 (M=Zn, Mg, Ca and Sr), with two different crystal structure groups were prepared using a solid-state reaction method, and their electronic band structures were investigated using Density Functional Theory (DFT) calculations and electrochemical measurement methods. Moreover, the dye-sensitized solar cell performance was also evaluated and, thereby, the effect of the electronic band structure on the photovoltaic properties was demonstrated.

2. Experimental section

2.1. Materials preparation

MWO_4 (M=Zn, Mg, Ca and Sr) powders were prepared using a conventional solid-state reaction method. The starting materials of ZnO, MgO, $CaCO_3$, $SrCO_3$ and WO_3 with 99.9% purity were purchased from High Purity Chemical (Osaka, Japan). Mixtures of the starting materials were homogenized by ball milling in ethanol for 24 h. The mixed slurries were dried in an oven (90 °C) and then calcined at 900 °C for 2 h in air.

2.2. Materials characterization

The crystal structures and phase purities of the calcined powders were examined by X-ray diffraction (XRD, M18XHF-SRA, MacScience, Yokohama, Japan). The powder morphology and size distributions were observed by field emission scanning electron microscopy (FESEM, JSM-6330F, JEOL, Tokyo, Japan), and the specific surface areas were measured using the BrunauerEmmettTeller method (BET, BELSORP-mini II, Bel, Osaka, Japan). The electrochemical measurements were performed using a potentiostat (CHI 608C, CH Instruments, Austin, TX, USA) in a conventional three electrode system with a platinum counter electrode and a saturated calomel reference electrode (SCE). In addition, the electronic band structures were calculated using the standard Cambridge serial total energy package (CASTEP) based on plane wave density functional theory (DFT). The kinetic energy cut-off was taken to be 300.0 eV, and the type of the exchange-correlation potential chosen was the generalized gradient approximation (GGA) [22] using the Perdew–Bruke–Ernzerhof (PBE) functional [23].

2.3. Photovoltaic performance

The sandwich-typed DSSCs were fabricated using a previously reported procedure [24]. The thicknesses of the metal tungstate films were measured by FESEM and the amounts of the dye adsorbed were quantified by UV–vis spectroscopy (Lambda 35, Perkin-Elmer, Waltham, MA, USA). The photovoltaic properties were examined using a potentiostat under an illumination of AM 1.5 with a solar simulator (Peccell Technologies; intensity: 100 mW cm^{-2}). Additionally, an electrochemical impedance analysis of the fabricated cells was also conducted using a potentiostat under illumination and by applying an open circuit voltage (V_{OC}) as the bias, in order to obtain information on the electric transport at the various interfaces [25].

3. Results and discussion

3.1. Crystal and electronic band structure

The schematic crystal structures of the divalent metal tungstates, MWO_4, with the wolframite structure (M=Zn and Mg) and scheelite structure (M=Ca and Sr) are presented in Fig. 1. The crystal structures are reconstructed from the previous data of the unit cell parameters and atomic positions [9,12]. Although they have a similar chemical formula, their structural environments are quite different. In metal tungstates with the wolframite structure, the tungsten (W) atom is octahedrally surrounded by six oxygen (O) atoms to form WO_6 octahedra, whereas metal tungstates with a scheelite structure exhibit a tetragonal structure consisting of WO_4 tetrahedra.

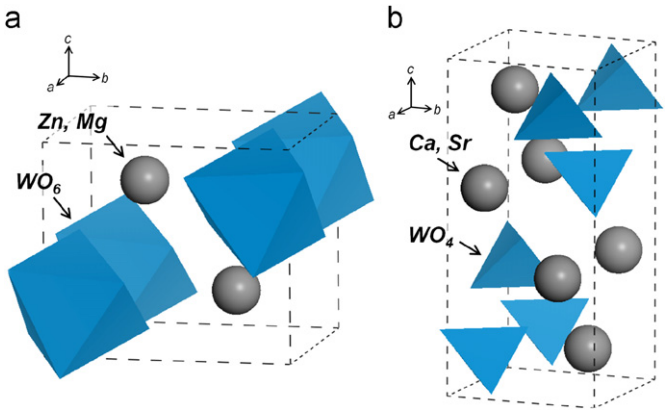

Fig. 1. Crystal structures of MWO_4: (a) wolframite structure (M=Zn, Mg) and (b) scheelite structure (M=Ca, Sr).

In order to predict the effects of the crystal structure on the electronic band structure in divalent metal tungstates, density functional theory (DFT) calculations were conducted. Fig. 2 shows the calculated electronic band structures and density of states (DOS) of the divalent metal tungstates. Upon the formation of the conduction band/valence band (CB/VB), the contribution of the elements was similar, i.e. the bottom of the CB mainly consisted of the W 5*d* orbitals and the top of the VB was predominantly composed of the O 2*p* orbitals. Although the contribution of each element is similar, $ZnWO_4$ (ZW), $MgWO_4$ (MW), $CaWO_4$ (CW) and $SrWO_4$ (SW) showed a wide range of band gap energies, viz. 2.95, 3.48, 4.25 and 4.58 eV, respectively, which were similar to the average values taken from previous studies [9,16,26–30]. These differences in the band gaps were attributed to the variations of the crystal field strength resulting from the different interactions between the orbitals of the W and O elements. The wolframite-structured metal tungstates (ZW and MW) appeared to have a longer W–O bond length (ZW=1.951 Å and MW=1.942 Å) in the WO_6 octahedra compared with those of the scheelite-structured metal tungstates (CW=1.782 Å and SW=1.779 Å), as summarized in Table 1. According to previous studies [7,10,11], the band gap in metal oxide compounds is strongly influenced by the crystal structure (e.g. metal–oxygen bond length), i.e. a longer bond length induces a weaker metal–oxygen orbital interaction and, thus, leads to a lower band gap. Therefore, the lower band gaps of the wolframite-structured metal tungstates were due to the weak band splitting, which originated from the longer bond length in the WO_6 octahedra than that in the scheelite structure.

On the other hand, another difference between the wolframite- and scheelite-structured metal tungstates was the configuration at the bottom of the CB and the top of the VB. Both ZW and MW showed relatively dispersive band structures compared with those of CW and SW. This indicates that the photogenerated charge carriers of the wolframite-structured metal tungstates have a smaller effective mass, leading to higher mobility [11]. As a result, it was confirmed that the electronic band structures in divalent metal tungstates are intimately related to their crystal structural environments.

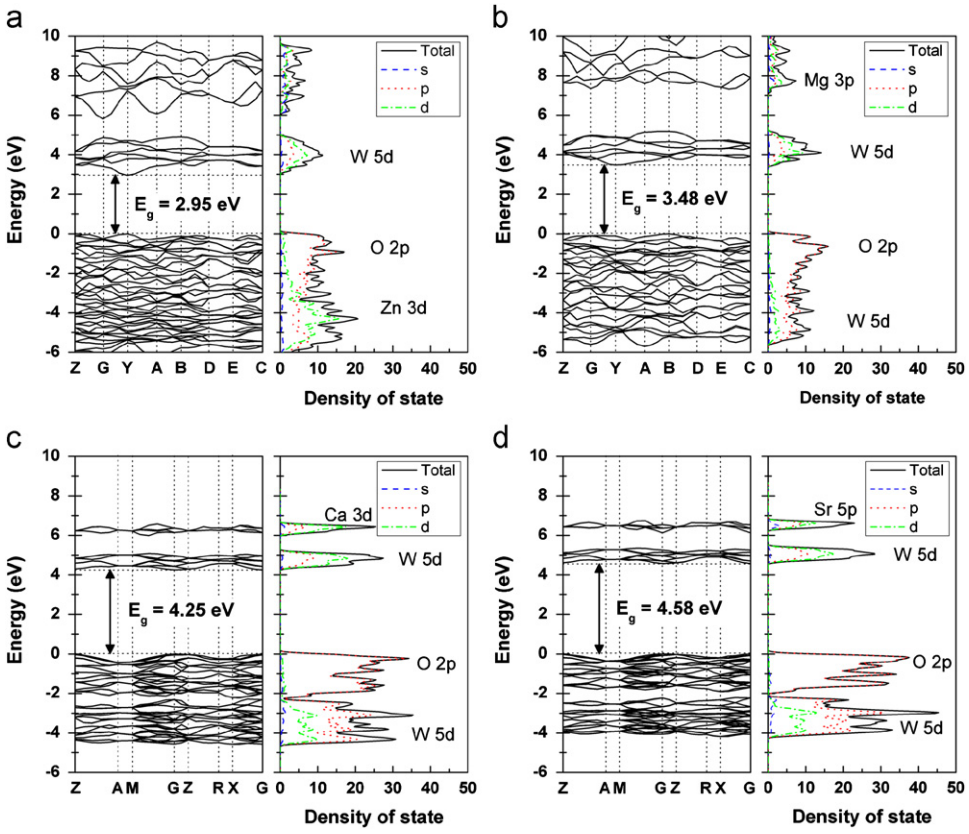

Fig. 2. Electronic band structures and density of states (DOS): (a) $ZnWO_4$, (b) $MgWO_4$, (c) $CaWO_4$ and (d) $SrWO_4$.

Table 1
Crystal structures and electronic band structures of divalent metal tungstates.

Compounds	Crystal structure	W–O bond length (Å)	Band gap (eV)		Flat band potential (V vs. SCE at pH 8)
			Calculated	Literature [9,16,26–30]	
$ZnWO_4$ (ZW)	Wolframite	1.951	2.95	3.65	−1.10
$MgWO_4$ (MW)		1.942	3.48	3.92	−1.02
$CaWO_4$ (CW)	Scheelite	1.782	4.25	4.54	−1.16
$SrWO_4$ (SW)		1.779	4.58	4.49	−1.24

Metal tungstate powders were practically synthesized and characterized in order to support the above results obtained by theoretical calculations. Fig. 3 shows the XRD patterns of the metal tungstate powders prepared by a solid-state reaction method. Each powder exhibited only a single phase, and all of the peaks were assigned to ZW, MW, CW and SW, as indexed in JCPDS Nos. 88-0251, 27-0789, 41-1431 and 08-0490, respectively. Additionally, the morphologies of the obtained powders were irregular, but their particle sizes were similar to each other, viz. approximately 1–3 μm (not shown here). There was also little difference in the BET surface area of the metal tungstate powders ($\sim 1\ m^2\ g^{-1}$).

Generally, the flat band potential (V_{fb}) is the potential required to flatten the band bending caused by the semiconductor–electrolyte junction, and it is a very useful parameter for the study of the electronic band structure. Hence, V_{fb} was measured by the electrochemical method for practical verification.

Fig. 4 shows the Mott–Schottky plots of the metal tungstate thick film electrodes in 1.0 M KCl (pH 8) electrolyte solution. Firstly, the measured V_{fb} values were −1.10, −1.02, −1.16 and −1.24 V vs. SCE for ZW, MW, CW and SW, respectively, all of which were negative. These negative values indicated that all of

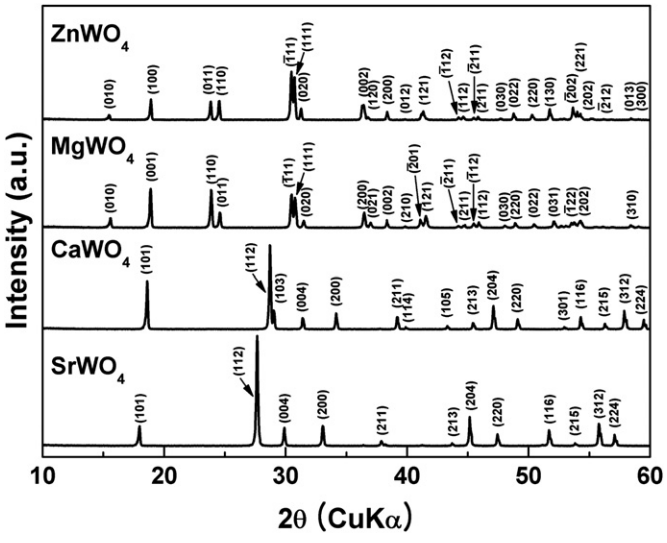

Fig. 3. X-ray diffraction patterns of MWO_4 (M=Zn, Mg, Ca and Sr) powders prepared by a solid-state reaction method.

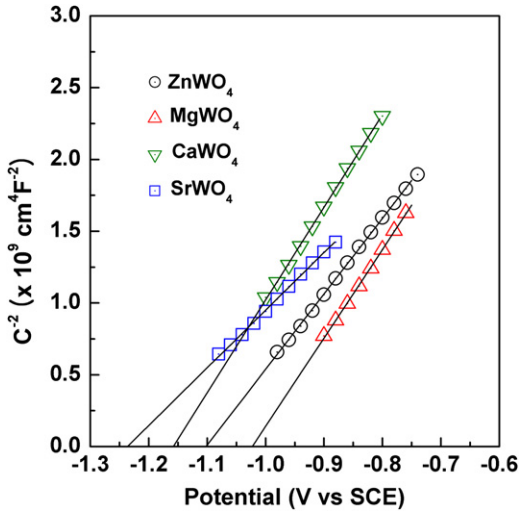

Fig. 4. Mott–Schottky plots of MWO_4 (M=Zn, Mg, Ca and Sr) electrodes in 1 M KCl electrolyte (pH 8) at a frequency of 1 kHz.

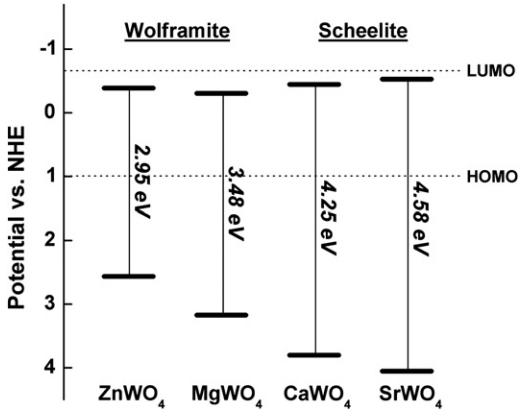

Fig. 5. Suggested electronic band structures of MWO_4 (M=Zn, Mg, Ca and Sr) compounds.

the synthesized divalent metal tungstates exhibited n-type semiconducting behavior. Furthermore, to facilitate the understanding of these divalent metal tungstates and for the purpose of comparison, the potential value vs. SCE should be converted to the potential vs. normal hydrogen electrode (NHE) by adding 0.242 V. Also, the linear pH dependence of V_{fb} with a slope of 0.059 V/pH was reported in previous studies [31] for most metal oxide semiconductors, which was attributed to the degree of protonation at the electrode surface. Using these relations, the V_{fb} values of ZW, MW, CW and SW were found to be −0.386, −0.306, −0.446 and −0.526 V vs. NHE at pH 0, respectively.

Assuming that the difference between the flat band potential and the CB edge potential is negligible for n-type semiconductors, the CB edge levels of the divalent metal tungstates can be obtained. On the basis of these V_{fb} values and the band gaps obtained from the DFT calculation, the overall band structures of the metal tungstates are described in Fig. 5. The lowest unoccupied molecular orbital (LUMO) and the highest occupied molecular orbital (HOMO) levels of the N719 dye molecule are also indicated [32], as shown in the figure; all of the CB levels of these compounds were observed to be positioned within the gap between the LUMO and the HOMO levels of the N719 dye molecule. Among them, the metal tungstates with the wolframite structure showed a relatively lower CB edge level than those with the scheelite structure, i.e. the CB edge levels were in the order of SW > CW > ZW > MW (lowest). This indicates that MW exhibited the highest potential difference (Δ) between the CB edge level and the LUMO level of N719 and, thus, a relatively higher driving force for electron injection from N719 to MW. On the contrary, the driving force for electron transfer from N719 to SW was the lowest. This is noteworthy for understanding the photoelectrochemical properties of these divalent metal tungstates.

3.2. Photovoltaic performance

DSSCs were fabricated using the prepared metal tungstate powders as the photoelectrodes and their photovoltaic properties were measured, in order to investigate the relationship between the electronic band structure and the photovoltaic/photoelectrochemical properties. Fig. 6 shows the photocurrent density–voltage (J–V) curves of the fabricated DSSCs. As summarized in Table 2, although all of the fabricated cells exhibited quite low photovoltaic performances, they were sufficient to investigate the difference in their photovoltaic properties. Moreover, these efficiency values could be further improved using nano-sized powders with a higher surface area. The photon energy conversion efficiency was observed to be in the order of ZW > MW > CW > SW. It was found that the DSSCs employing the metal tungstates with the wolframite structure (ZW and MW) exhibited better performance than those with the scheelite structure (CW and SW). Basically, the role of the semiconductor layer in the DSSC is to assist the electron transport from the dye molecules to the transparent conducting oxide (TCO), i.e. the electron injection and collection process, and thus the electronic band structure is an important factor for achieving a higher cell performance. Therefore, the cell efficiency is bound to be affected by the above factors, for example the CB edge level and the dispersive band structure.

The measured cell efficiency showed somewhat different results compared with the trend of the CB edge level. Accordingly, an

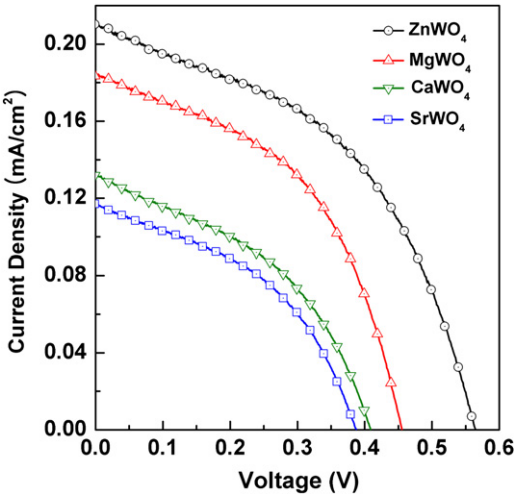

Fig. 6. J–V characteristics of the DSSCs employing the synthesized divalent metal tungstate photoelectrodes.

Table 2
Photovoltaic parameters of DSSCs employing MWO_4 (M=Zn, Mg, Ca and Sr) photoelectrodes.

Semiconductors	V_{OC} (V)	J_{SC} (mA cm^{-2})	FF	Eff (%)	ω_{max} in R_3 (Hz)
$ZnWO_4$ (ZW)	0.57	0.21	0.459	0.054	3.74
$MgWO_4$ (MW)	0.46	0.18	0.429	0.036	4.54
$CaWO_4$ (CW)	0.41	0.13	0.422	0.023	3.74
$SrWO_4$ (SW)	0.39	0.12	0.433	0.020	3.74

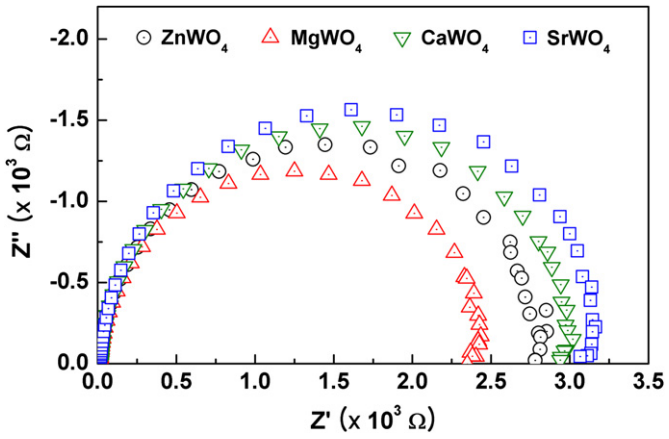

Fig. 7. Electrochemical impedance spectra of MWO_4-based DSSCs (M=Zn, Mg, Ca and Sr).

additional electrochemical impedance spectrum analysis was performed to further understand the difference in the charge transfer and the charge recombination rate. Fig. 7 presents the Nyquist plots of the DSSCs employing the divalent metal tungstates. Generally, the impedance components in a DSSC are observed in the frequency ranges of $10^3 \sim 10^5$ Hz (ω_1 or ω_2), 1–10^3 Hz (ω_3) and 0.1–1 Hz (ω_4). These components are assigned to the impedances (R) at the TCO/semiconductor (ω_1), counter electrode/electrolyte (ω_2) and semiconductor/dye/electrolyte (ω_3) interfaced, and that caused by the diffusion of the electrolyte (ω_4) [25]. It was observed that the measured value of R_3 (at ω_3) gradually decreased in the order of SW, CW, ZW and MW. The decrease in R_3 was attributed to the increase in the injected electron density resulting from the adsorbed N719 dye molecules, due to the higher Δ between the CB edge level and the LUMO level. Therefore, although MW seemed to be a favorable material to be used as the photoelectrode from the viewpoint of electron injection, the ZW-based DSSC showed higher performance than the MW-based DSSC. These results could be additionally explained by another factor affecting the photovoltaic performance, namely the maximum frequency (ω_{max}) in R_3 is inversely proportional to the electron lifetime (τ) [25,33]. The ω_{max} value of the MW-based DSSC was relatively higher (i.e. shorter electron lifetime), as shown in Table 2, which indicates that the recombination rate of injected electrons is higher. Consequently, the higher photovoltaic performance for the ZW-based DSSC was considered to originate from its electronic properties, such as the higher driving force for the electron injection process and lower electron recombination rate.

Overall, the electronic band structure and photovoltaic properties of DSSCs are closely related to each other and, moreover, the photovoltaic performance can be adjusted and improved by controlling the crystal structure and electronic band structure of the semiconductor materials.

4. Conclusion

Divalent metal tungstates with wolframite and scheelite structures were successfully prepared and their electronic band structures were characterized. From the electronic band calculation, the wolframite-structured metal tungstates exhibited comparatively smaller band gaps of 2.95 and 3.48 eV for $ZnWO_4$ and $MgWO_4$, whereas the scheelite-structured metal tungstate exhibited much larger band gaps of 4.25 and 4.58 eV for $CaWO_4$ and $SrWO_4$, respectively; this was attributed to their different crystal structural environments, such as their W–O bond lengths. Also, the overall band structures were described with the aid of the flat band potential values and indicated that the metal tungstates with the wolframite structure had lower conduction band edge levels than those with the scheelite structure. On the basis of the electronic band structure analysis, the metal tungstates were used as the working electrodes for DSSCs and the resulting energy conversion efficiencies were found to be in the order of $ZnWO_4 > MgWO_4 > CaWO_4 > SrWO_4$. The relatively higher DSSC performance of the metal tungstates with the wolframite structure, especially $ZnWO_4$, was attributed to their efficient electron transfer, i.e. higher electron injection and lower electron recombination rates.

Acknowledgment

This work was supported by the National Research Foundation of Korea (NRF) grant funded by the Korean government (MEST) (2009-0092779) and this work was also supported by the Nano R&D program through the National Research Foundation of Korea funded by MEST (2009-0082659) and the research program 2009 of the Kookmin University in Korea.

References

[1] M.R. Hoffmann, S.T. Martin, W. Choi, D.W. Bahnemann, Chem. Rev. 95 (1995) 69–96.
[2] A. Kudo, Int. J. Hydrogen Energy 32 (2007) 2673–2678.
[3] M. Gratzel, Nature 414 (2001) 338–344.
[4] S. Burnside, J.-E. Moser, K. Brooks, M. Gratzel, J. Phys. Chem. B 103 (1999) 9328–9332.
[5] B. Tan, E. Toman, Y. Li, Y. Wu, J. Am. Chem. Soc. 129 (2007) 4162–4163.
[6] T. Lana-Villarreal, G. Boschloo, A. Hagfeldt, J. Phys. Chem. C 111 (2007) 5549–5556.
[7] I.-S. Cho, C.H. Kwak, D.W. Kim, S. Lee, K.S. Hong, J. Phys. Chem. C 113 (2009) 10647–10653.
[8] J.Y. Kim, S.B. Choi, D.W. Kim, S. Lee, H.S. Jung, J.-K. Lee, K.S. Hong, Langmuir 24 (2008) 4316–4319.
[9] Z. Shan, Y. Wang, H. Ding, F. Huang, J. Mol. Catal. A—Chem. 302 (2009) 54–58.
[10] S. Ouyang, Z. Li, Z. Ouyang, T. Yu, J. Ye, Z. Zou, J. Phy. Chem. C 112 (2008) 3134–3141.
[11] S. Ouyang, N. Kikugawa, D. Chen, Z. Zou, J. Ye, J. Phys. Chem. C 113 (2009) 1560–1566.
[12] S.H. Yoon, D.-W. Kim, S.-Y. Cho, K.S. Hong, J. Eur. Ceram. Soc. 26 (2006) 2051–2054.
[13] R.C. Pullar, S. Farrah, N.McN. Alford, J. Eur. Ceram. Soc. 27 (2007) 1059–1063.
[14] A.K. Bhattacharya, R.G. Biawas, A. Hartridge, J. Mater. Sci. 32 (1997) 353–356.
[15] D.S. Kim, M. Ostromecki, I.E. Wachs, J. Mol. Catal. A—Chem. 106 (1996) 93–102.
[16] H. Fu, J. Lin, L. Zhang, Y. Zhu, Appl. Catal. A—Gen. 306 (2006) 58–67.
[17] G. Huang, Y. Zhu, Mat. Sci. Eng. B 139 (2007) 201–208.
[18] N. Faure, C. Borel, M. Couchaud, G. Basset, R. Templier, C. Wyon, Appl. Phys. B 63 (1996) 593–598.
[19] A.A. Kaminskii, H.J. Eichler, K.-I. Ueda, N.V. Klassen, B.S. Redkin, L.E. Li, J. Findeisen, D. Jaque, J. Garcia-Sole, J. Fernandez, R. Balda, Appl. Optics 38 (1999) 4533–4547.
[20] X. Zhao, W. Yao, Y. Wu, S. Zhang, H. Yang, Y. Zhu, J. Solid State Chem. 179 (2006) 2562–2570.
[21] P.K. Pandey, N.S. Bhave, R.B. Kharat, Mater. Lett. 59 (2005) 3149–3155.
[22] J.A. White, D.M. Bird, Phys. Rev. B 50 (1994) 4954–4957.
[23] J.P. Perdew, K. Burke, M. Ernzerhof, Phys. Rev. Lett. 77 (1996) 3865–3868.
[24] H.S. Jung, J.-K. Lee, S. Lee, K.S. Hong, H. Shin, J. Phys. Chem. C 112 (2008) 8476–8480.
[25] T. Hoshikawa, M. Yamada, R. Kikuchi, K. Eguchi, J. Electrochem. Soc. 152 (2005) E68–E73.
[26] R. Lacomba-Perales, J. Ruiz-Fuertes, D. Errandonea, D. Martinez-Garcia, A. Segura, EPL 83 (2008) 37002.
[27] M. Bonanni, L. Spanhel, M. Lerch, E. Fuglein, G. Muller, Chem. Mater. 10 (1998) 304–310.
[28] S.K. Arora, B. Chudasama, Crys. Res. Technol. 41 (2006) 1089–1095.
[29] Y. Zhang, N.A.W. Holzwarth, R.T. Williams, Phys. Rev. B 57 (1998) 12738–12750.
[30] V.B. Mikhailik, H. Kraus, D. Wahl, M. Itoh, M. Koike, I.K. Bailiff, Phys. Rev. B 69 (2004) 205110.
[31] H. Gerischer, in: H. Eyring, D. Henderson, W. Jost (Eds.), Physical Chemistry: An Advanced Treatise, vol. IXA, Academic Press, New York, 1970.
[32] S. Gubbala, V. Chakrapani, V. Kumar, M.K. Sunkara, Adv. Funct. Mater. 18 (2008) 2411–2418.
[33] J. van de Lagemaat, N.-G. Park, A.J. Frank, J. Phys. Chem. B 104 (2000) 2044–2052.